JACS
JOURNAL OF THE AMERICAN CHEMICAL SOCIETY
Article
pubs.acs.org/JACS

Surface-assisted Dehydrogenative Homocoupling of Porphine Molecules

Alissa Wiengarten,[†] Knud Seufert,[†,⊥] Willi Auwärter,*[,†,‡] David Ecija,[†,#] Katharina Diller,[†,$] Francesco Allegretti,[†] Felix Bischoff,[†] Sybille Fischer,[†] David A. Duncan,[†] Anthoula C. Papageorgiou,[†] Florian Klappenberger,[†] Robert G. Acres,[§] Thien H. Ngo,[∥] and Johannes V. Barth[†]

[†]Physik Department E20, Technische Universität München, James-Franck-Straße 1, D-85748 Garching, Germany

[‡]Institute for Advanced Study, Technische Universität München, Lichtenbergstrasse 2a, D-85748 Garching, Germany

[§]Elettra-Sincrotrone Trieste, Strada Statale 14, km 163.5, 34149 Basovizza, Trieste, Italy

[∥]International Center for Young Scientists (ICYS-MANA), National Institute for Materials Science (NIMS), 1-2-1 Sengen, Tsukuba-city. Ibaraki 305-0047, Japan

Supporting Information

ABSTRACT: The templated synthesis of porphyrin dimers, oligomers, and tapes has recently attracted considerable interest. Here, we introduce a clean, temperature-induced covalent dehydrogenative coupling mechanism between unsubstituted free-base porphine units yielding dimers, trimers, and larger oligomers directly on a Ag(111) support under ultrahigh-vacuum conditions. Our multitechnique approach, including scanning tunneling microscopy, near-edge X-ray absorption fine structure and photoelectron spectroscopy complemented by theoretical modeling, allows a comprehensive characterization of the resulting nanostructures and sheds light on the coupling mechanism. We identify distinct coupling motifs and report a decrease of the electronic gap and a modification of the frontier orbitals directly associated with the formation of triply fused dimeric species. This new on-surface homocoupling protocol yields covalent porphyrin nanostructures addressable with submolecular resolution and provides prospective model systems towards the exploration of extended oligomers with tailored chemical and physical properties.

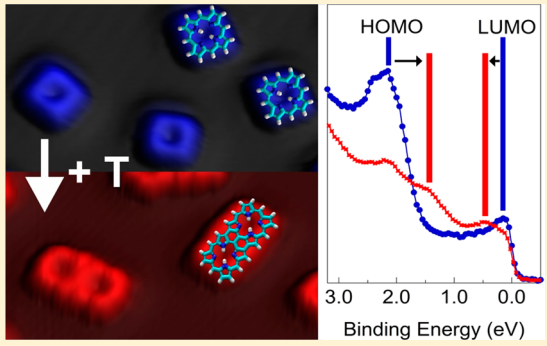

INTRODUCTION

Porphyrin molecules play a decisive role in many important biological processes[1−3] and have been investigated extensively in solution and on surfaces.[4−14] Thanks to the chemical versatility and the flexibility of the molecular modules, they have increasingly contributed to applications in hybrid molecular and photovoltaic devices.[15−17] Recently, a variety of porphyrin building blocks has been employed for the construction of differently conjugated molecular wires, tapes, rings, and discrete oligomeric arrays.[18−21] Such artificial low-dimensional, covalently linked nanostructures have great promise for molecular electronics, optoelectronics, gas sensing,[22] and light-harvesting,[18] featuring a steadily decreasing band gap as a function of the tape length[4,7] while at the same time exhibiting interesting nonlinear optical properties.[23,24] Porphyrin dimers, representing the smallest possible porphyrin oligomer, have attracted special attention for example as theoretically accessible model systems for energy transfer studies[20] or molecule-sized memory units for many-valued logic.[21] Porphyrin oligomers are usually synthesized and handled in solution. However, in order to develop nanostructures or device architectures suitable for future applications, it is necessary to immobilize these oligomers onto an appropriate supporting substrate or integrate them in well-defined environments. In addition, a molecular-level characterization is greatly facilitated by employing atomistically clean interfaces under ultrahigh-vacuum (UHV) conditions. To this end, pioneering studies used scanning probe microscopy to image spray-deposited porphyrin oligomers with limited resolution.[25,26] As sublimation is restricted to short oligomers[27,28] and spray deposition has practical limitations, the on-surface synthesis of covalently linked porphyrin architectures under UHV has recently come into focus.[29−32] Typically precursor molecules are sublimated onto a support, and subsequent annealing allows one to overcome the activation barriers to form covalent linkages. Often the covalent coupling sites are tailored by substituting hydrogen with halogen atoms for Ullmann coupling; these substituents provide suitable leaving groups, allowing the porphyrin molecules to more easily form direct C−C bonds.[31] A major disadvantage of this approach is the frequent generation of spurious byproducts remaining on the surface as contaminants.

Received: February 17, 2014
Published: June 23, 2014

   dx.doi.org/10.1021/ja501680n | J. Am. Chem. Soc. 2014, 136, 9346−9354

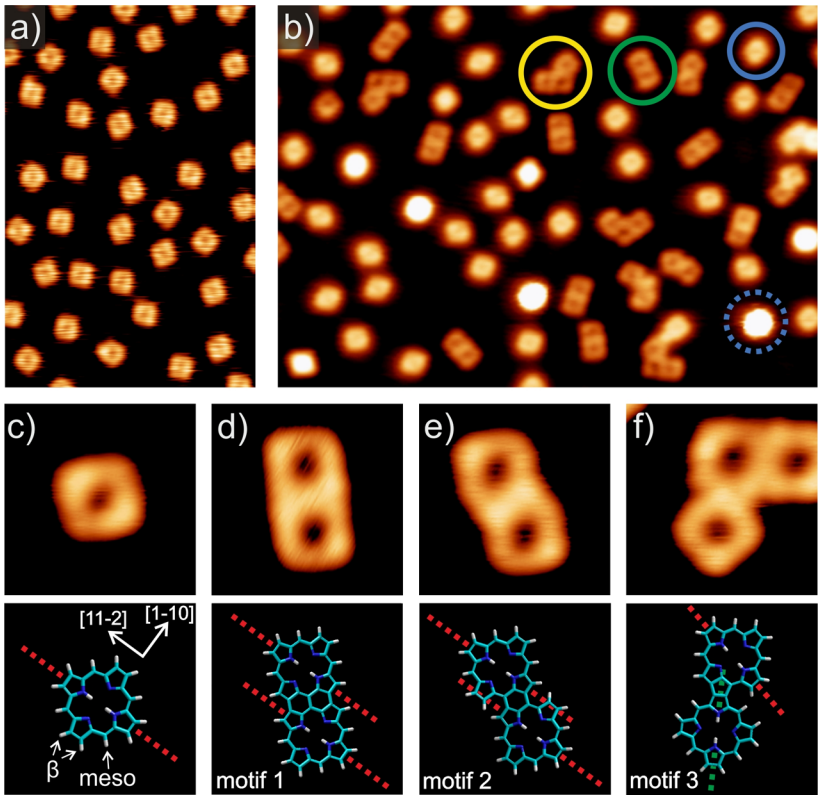

Figure 1. STM data on 2H-P and homocoupling products. (a) Random distribution of individual 2H-P on Ag(111) after deposition at a sample temperature T_S of 345 K (13.0 × 19.8 nm^2, −0.8 V, 0.2 nA). (b) Overview image after annealing a 2H-P multilayer, grown at room temperature, to T_S = 573 K. The colored circles highlight distinct species: monomer (blue), dimer (green), and trimer (yellow). The bright features (dashed circle) are assigned to porphines interacting with Ag adatoms (28.0 × 19.8 nm^2, −0.2 V, 0.1 nA). (c) 2H-P monomer with structural model and first symmetry axis (red dotted line). Directions of the Ag(111) substrate are indicated in white. (d–f) Three different binding motifs for oligomers with corresponding structural models and symmetry axes (2.5 × 2.5 nm^2, −0.15 V, 0.12 nA). C, N, and H atoms are indicated in cyan, blue, and white, respectively. (d) Binding motif 1 of triply fused dimer: *β-β*, *meso-meso*, *β-β* (positions are labeled and marked by arrows in c). (e) Binding motif 2 of doubly fused dimer: *meso-β*, *β-meso*. (f) Binding motif 3: *β-β*, *meso-β*.

Porphine, the simplest possible porphyrin species consisting solely of the tetrapyrrole macrocycle, has been comprehensively studied on metal surfaces[33−37] and is the most abundant building block for porphyrin tapes in solution.[23,38,39] In this study we demonstrate the surface-assisted covalent coupling between free-base porphines (2H-P) on a Ag(111) substrate proceeding without reaction byproducts left on the surface. By thermal activation only, the homocoupling reaction results in the formation of a variety of dimers and larger oligomers. Moreover, we use the relatively unreactive Ag(111) surface to prevent the expression of coordination bonds with adatoms, as observed by Haq et al. on the Cu(110) surface.[35] A high yield of triply fused dimers and longer oligomers is achieved by heating the substrate during deposition. This finding adumbrates the formation of porphine tape[18,40−42] analogues. To comprehensively characterize the chemical, geometric, and electronic structure of in situ prepared covalently linked porphine molecules on Ag(111), a multimethod approach[43] consisting of constant current mode and dI/dV mapping scanning tunneling microscopy (STM), ultraviolet photoelectron spectroscopy (UPS), X-ray photoelectron spectroscopy (XPS), and near-edge X-ray absorption fine structure (NEXAFS) spectroscopy measurements, complemented by density functional theory (DFT) calculations, was utilized.

From a more general perspective, our study introduces an on-surface reaction mechanism for macrocyclic species, namely the homocoupling, to covalently link single functional molecules on metallic supports and thus contributes to the ongoing intense research efforts aiming for robust nanoarchitectures synthesized on solid surfaces. This holds promise for significant developments in the fields of nanoscience and nanotechnology.[44−48] The linking of single functional molecules is a crucial aspect for tailoring the structure, stability, and functionality of the resulting assemblies. Therefore, control of the intermolecular interactions and aggregation processes is a major aim of molecular nanoscience. Self-assembled structures—stabilized by van der Waals interactions, hydrogen bonds, and metal−organic coordination bonds—can be engineered with a high degree of perfection and reproducibility.[10,49] More recently, by interconnecting functional molecules through covalent bonds, robust low-dimensional architectures were formed on surfaces.[32,45,47,50−52] In contrast to previous studies, our approach yields directly linked macrocycles to form extended conjugated π systems without requiring special leaving groups or substituents.

■ EXPERIMENTAL AND COMPUTATIONAL DETAILS

The Ag(111) crystal was prepared by repeated cycles of Ar^+ sputtering and annealing to 720 K. Porphine molecules (Frontier Scientific, purity >95%) were deposited via organic molecular beam epitaxy from a quartz crucible held typically at T_{cru} = 473 K, resulting in a deposition rate of roughly 0.02 monolayer (ML)/min, where a ML is defined as a full surface coverage by 2H-P.[36] It has to be noted that efforts to increase the 2H-P deposition rate by increasing the

dx.doi.org/10.1021/ja501680n | J. Am. Chem. Soc. 2014, 136, 9346−9354

temperature proved problematic, in contrast to experiments performed on various *meso*-substituted porphyrins. Higher crucible temperatures resulted in nonreproducible deposition rates, decreasing with time. This effect is tentatively assigned to a polymerization of the 2H-P powder in the crucible. The specific substrate temperatures T_S during sample preparation are indicated in the text and in the figure captions.

The STM experiments were carried out in a custom-designed UHV system equipped with a low-temperature CreaTec-STM (www.lt-stm.com). For all measurements, the sample was held at 6 K and the system base pressure was below 5×10^{-10} mbar. The STM images were acquired in constant current mode with an electrochemically etched tungsten tip and the bias applied to the sample. The dI/dV maps were recorded simultaneously with the topographic images using an internal lock-in amplifier (V_{rms} = 18 mV, f = 2.97 kHz).

The UPS measurements were performed at the Materials Science beamline of the ELETTRA storage ring in Trieste, Italy. The end station consists of a UHV surface science chamber that operates at a base pressure of 2×10^{-10} mbar and is equipped with standard facilities for sample manipulation and characterization. All measurements were performed at room temperature, using a SPECS PHOIBOS 150 electron energy analyzer of 150 mm mean radius fitted with a 1D-DLD detector. Linearly polarized radiation was used, and all spectra were recorded using a photon energy of 30 eV. The energy resolution of the measurements was about 0.13 eV, and the electron detection geometry was varied between normal and grazing emission (60° off-normal, corresponding to normal incidence of the photon beam) with an acceptance angle of ±7°. The UPS measurements were complemented by XPS (Figure SI 6, Supporting Information) and NEXAFS data, in order to assess the cleanliness, chemical state, coverage, and molecular orientation in differently prepared layers.

The NEXAFS data presented in Figure 4 were recorded at the HE-SGM beamline at the BESSY II storage ring (Berlin, Germany) in the partial electron yield mode (PEY) using a retarding voltage of −150 V. The experiments were performed in UHV, with base pressures in the low 10^{-9}–10^{-10} mbar regime. For each of the three recorded incidence angles between the surface normal and the electric field vector of the linearly polarized light the photocurrent signal of a contaminated gold grid traversed by the X-ray beam was recorded simultaneously with the PEY spectra. After the energy scale was referenced against a characteristic peak at 285 eV of the gold grid spectrum, the signal of a bare Ag(111) crystal was subtracted from the sample spectrum, followed by a correction for the photon flux and a normalization of the edge jump to one.[53]

The DFT calculations of the electronic structure of a porphine monomer and a symmetric dimer (cf. Figure 4a,b) were performed using the software package StoBe,[54] which describes the Kohn–Sham orbitals by a linear combination of Gaussian type orbitals. A revised Perdew, Burke, and Ernzerhof (RPBE) exchange-correlation functional[55,56] was used for all calculations, which were conducted for isolated molecules without taking the surface into account. In a first step the geometries of the molecules were optimized using all-electron triple-ζ plus valence polarization type basis sets for the description of nitrogen,[57] carbon,[57] and hydrogen[58] atoms. For both molecules the optimization resulted in a flat geometry: i.e., the pyrrolic subunits shared the same plane. The same basis sets were used for deriving the ground state properties shown in Figure 5e. NEXAFS simulations were performed using a double basis set technique within the transition potential method.[59,60] Details on the simulation of the NEXAFS and XPS data are described in the Supporting Information (Figures SI 4 and SI 6).

RESULTS AND DISCUSSION

Interfacial Homocoupling Scenario. In agreement with previously published work,[36] depositing small amounts of porphine molecules onto the Ag(111) substrate held at T_S = 345 K resulted in a submonolayer (sub-ML) coverage of dispersed, flat-lying monomers (Figure 1a). Figure 1c shows a single 2H-P molecule whose shape is essentially squarelike with a depression in the center. Two brighter protrusions in two opposing corners break the 4-fold symmetry and define the first symmetry axis of the porphine (dotted line in Figure 1c, lower panel). The resulting 2-fold symmetry of the molecule on the surface is induced by the two central hydrogen atoms.[36] The second symmetry axis, given by the two darker lobes, is aligned along one of the three close-packed $\langle 1\bar{1}0 \rangle$ directions of the underlying Ag(111) surface. Due to repulsive interactions, the porphine molecules do not form any aggregates or islands on Ag(111) at low sub-ML coverages.[36]

To trigger the covalent linking between porphine molecules, two approaches were used. In the first approach, a multilayer of 2H-P was grown on the Ag(111) substrate at T_S = 300 K. Subsequent annealing to 573 K induces desorption of molecules of weakly bound layers and yields a sub-ML coverage (Figure 1b). This step affords monomers (marked by a blue circle in Figure 1b), covalently linked dimers (Figure 1b (green circle),d,e), trimers (yellow circle in Figure 1b and Figure SI 1 (Supporting Information)), and more extended porphine oligomers.

The dimerization process is described by the formal reaction equation $2C_{20}N_4H_{14} \rightarrow C_{40}N_8H_{28-2n} + nH_2$ with n = 2, 3 (vide infra).

The high-resolution images in Figure 1d–f reveal that the porphine coupling —yielding the oligomers—results in three distinct motifs between 2H-P units. Motif 1, in Figure 1d, has a center-to-center distance of 8.5 ± 0.3 Å, which is significantly less than the 10.8 Å observed by Haq et al. for Cu-mediated porphine dimers on the Cu(110) surface.[35] Thus, linking via silver adatoms can be excluded, implying that the mechanism for oligomerization is the formation of covalent C–C bonds by dehydrogenation. Geometry optimization, based on the semiempirical AM1 method in the framework of the HyperChem package,[61] indeed yields a center-to-center distance of 8.5 Å for an isolated dimer (Figure 1d, lower panel) linked with covalent C–C bonds, in excellent agreement with the experimental observations. The same value was obtained by the geometry optimization carried out with the DFT code StoBe (Figure 4b). These values are also consistent with the calculated distances reported for C–C covalently coupled porphine oligomers (8.9 Å,[35] 8.4 Å[62]), which are significantly less than those from gas-phase molecular mechanics calculations of two aligned 2H-P molecules. Since the only reaction byproduct is hydrogen, which desorbs from the surface at these temperatures, this mechanism yields a clean surface, in contrast to many reactions involving halogen byproducts (e.g., see refs 31, 63, and 64). The binding in motif 1 (*β-β*, *meso-meso*, *β-β*; positions are labeled and marked by arrows in Figure 1c, lower panel) is attributed to the dehydrogenation of three neighboring carbon atoms per molecule and the formation of three covalent C–C bonds, as implied by the edges of the two porphine units being collinear, resulting in straight oligomers (see Figure 1d and Figure SI 1 (Supporting Information)). Analogously, in agreement with structural models obtained with HyperChem, motif 2 (*meso-β*, *β-meso*) is assigned to the dehydrogenation of two carbon atoms per molecule forming two covalent C–C bonds, as there is a slight lateral offset of 2.2 ± 0.5 Å between the two 2H-P molecules. For motifs 1 and 2 the constituent porphine units are oriented along the same direction with respect to the underlying substrate, as evidenced by the two protrusions defining the first symmetry axis. Within the precision of the STM measurement (±5°) the symmetry axes coincide with those of the 2H-P monomers. Thus, even in

the oligomers, the porphine units are aligned with the three close-packed directions of the Ag(111) substrate. Consequently, six equivalent orientations of straight triply fused dimers and oligomers are observed in the STM data.

Binding motif 3 (*β-β, meso-β*) is associated with two covalent C−C bonds (Figure 1f), due to strong agreement with the structural model (Figure 1f, lower panel). Consistently, models based on a single C−C bond deviate significantly from the experimentally observed arrangement. In contrast to the binding motifs 1 and 2, the two constituting units exhibit different orientations in motif 3. The symmetry axes of the 2H-P molecules in Figure 1f (dotted lines) do not form an angle of 60°, as might be expected from the preference of porphines to align along the high symmetry directions of the surface, but instead an angle of approximately 45°. Hence, in motif 3 one symmetry axis deviates by 15° from the dense-packed substrate directions. The fact that this adsorption configuration is not preferred for individual 2H-P molecules but is frequently observed in the oligomers implies that the energy gain by the covalent bonds establishing the oligomers overcompensates the reduced binding energy due to a nonideal registry to the Ag(111) lattice: i.e., the covalent interactions prevail over site-specific molecule−substrate interactions. Consequently, the substrate geometry does not dictate the conformation of the oligomers, as confirmed by preliminary data on Ag(100) evidencing similar oligomeric structures.

In addition to the monomers and oligomers, bright species with lateral dimensions of a single 2H-P molecule are observed after annealing (marked with a dotted blue circle in Figure 1b), which we assign to the tetrapyrrole macrocycle reacting with silver surface atoms. As shown in Figure SI 2 (Supporting Information), dimers and oligomers were observed to react with surface atoms as well.

Using this first experimental approach with an annealing time of 20 min, 49 ± 2% of all porphines was incorporated in oligomers. A prolongation of the annealing time led to a moderate increase in the area density of oligomers; however, this process is not efficient, as the number of available reactants continuously decreases due to monomer desorption (desorption rate at 533 K: ∼3% ML/min). For example, a doubling of the time (from 10 to 20 min) increased the dimer density by only 16%. Accordingly, as evident from Figure 1b, the average oligomer length (2.1 ± 0.3 porphine units) and the oligomer coverage (0.11 ± 0.02 ML of 2H-P) are rather limited.

To circumvent this problem, aiming for an increased amount of oligomers, we introduced a second experimental approach, where the porphine molecules were deposited onto a sample held at elevated temperatures. Here, the continuous supply of reactants counteracts the desorption of monomers. In the process, three different substrate temperatures T_S were applied (533, 573, and 613 K; cf. Figure 2), while the deposition time was 90 min in all three cases. After deposition at T_S = 533 K a sub-ML coverage was observed consisting of isolated monomers, dimers, and a few larger oligomers (Figure 2a). Despite using a temperature reduced by 40 K in comparison to the first approach, the oligomer coverage (0.3 ± 0.04 ML) clearly exceeds that achieved by the first approach. Increasing the sample temperature during deposition to the same temperature used in the first approach (573 K) augments the percentage of molecules bound in oligomers in comparison to the first approach (from 49% to 80%). After deposition at 613 K, oligomers consisting of more than 90 porphine units were observed and the average oligomer size increased considerably (from 2.1 to 8.2 porphine units; see Table 1), while still guaranteeing a high surface coverage of oligomers of 33% (Figure 2d). Table 1 summarizes the statistical analysis of the oligomerization for the three temperatures T_S. Specifically, the average oligomer size and the proportion of molecules bound in oligomers increases considerably with T_S, whereas the oligomer coverage is only marginally affected.

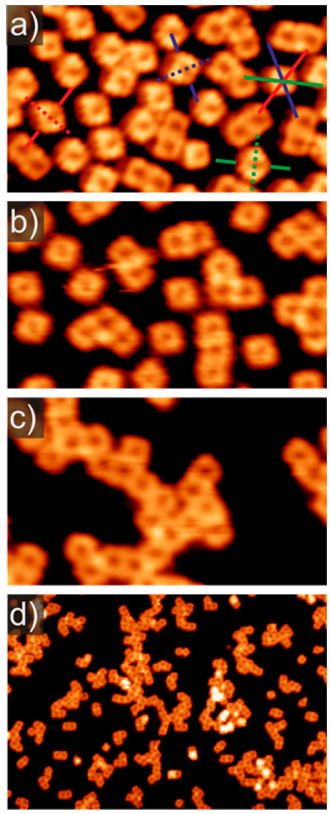

Figure 2. STM micrographs of homocoupling reaction products on the Ag(111) substrate held at different temperatures T_S during deposition: (a) 533 K; (b) 573 K: (c, d) 613 K. The solid lines indicate the close-packed $\langle 1\bar{1}0 \rangle$ directions of the crystal, and the dashed lines indicate the $\langle 11\bar{2} \rangle$ directions. Image sizes: (a−c) 12.6 × 7.3 nm^2; (d) 46.1 × 31.2 nm^2. Image parameters: (a) −0.5 V, 3 nA; (b) −1.8 V, 0.07 nA; (c) −1 V, 0.09 nA; (d) −0.7 V, 0.1 nA.

Table 1. Average Oligomer Length (in Porphine Units; the Error Corresponds to the Standard Deviation), with the Coverage of Monomers and Oligomers and Occurrence of Different Binding Motifs in Percent of Reacted Molecules as a Function of the Substrate Temperature T_S during Deposition[a]

	substrate temperature T_s		
	533 K	573 K	613 K
average oligomer length	2.1 ± 0.3	2.7 ± 1.3	8.2 ± 10.8
coverage	59 ± 4	45 ± 4	34 ± 4
monomer coverage	29 ± 4	9 ± 2	1 ± 0.5
oligomer coverage	30 ± 4	35 ± 3	33 ± 3
percentage of nonmonomers	51 ± 2	80 ± 3	97 ± 3
binding motif 1	81 ± 5	74 ± 5	67 ± 6
binding motif 2	13 ± 3	12 ± 3	14 ± 5
binding motif 3	6 ± 3	14 ± 3	20 ± 5

[a]All coverages are given in percent of 1 ML of 2H-P on Ag(111) as defined by Bischoff et al.[36]

dx.doi.org/10.1021/ja501680n | J. Am. Chem. Soc. 2014, 136, 9346−9354

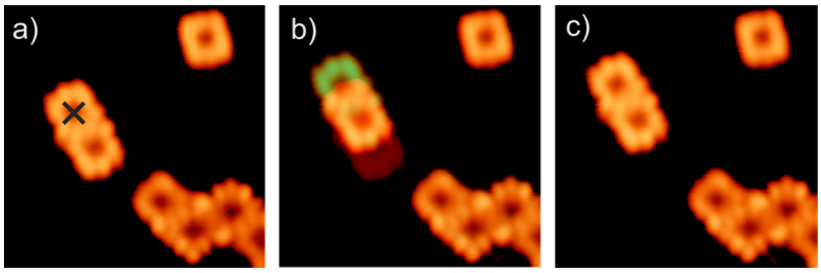

Figure 3. Stability of a dimer. A voltage pulse applied at the position marked by the black cross in the STM image in (a) results in a concerted lateral translation of the dimer entity depicted in the STM image in (c). In (b) a superposition of the STM images before (red hue) and after (green hue) the dimer lateral manipulation is shown to highlight the change in position (5.2 × 5.2 nm^2, −0.3 V, 0.2 nA).

Thus, when the two approaches are compared, the second leads to a higher oligomer coverage which is nearly independent of the temperature T_S, and by increasing T_S the average oligomer length is increased.

For all oligomers resulting from this second approach, we identified exclusively the three binding motifs introduced before for the first approach (Figure 1d–f). A statistical analysis yields a clear prevalence of motif 1 based on three C–C bonds over motifs 2 or 3 based on only two C–C bonds at all three temperatures (see Table 1). Intriguingly, the percentage of the triply fused motif 1 decreases with increasing temperature from 81 ± 5% (T_S = 533 K) to 67 ± 6% (T_S = 613 K). Binding motif 2 shows no pronounced temperature dependence, while motif 3 becomes more likely with increasing temperature (see Table 1). On first sight, this seems counterintuitive, as the formation of motif 1 involves the scission of six C–H bonds, in comparison to only four in the case of motifs 2 and 3. Furthermore, the probability for two 2H-P monomers to congregate in a perfectly collinear, centered fashion (motif 1) is lower than the probability to meet with a lateral offset (motif 2). In addition, conceivable dimers stabilized by a single C–C bond (*β-β*, motif 3*), resulting in a lateral displacement exceeding that of motif 2, were never observed. Within the precision of the modeling, none of the coupling motifs allows for a commensurate adsorption of all units in an oligomer on the Ag(111) lattice. Consequently, we discard the surface registry as the exclusive driving force for the preference of motif 1 and the absence of motif 3*. There are two tentative explanations for the above observations. First, in a traditional wet chemistry approach, triply fused tapes and arrays are typically achieved via singly *meso-meso* linked oligomer intermediates,[26,39] benefiting from the relative lability of the *meso*-C–H bond in comparison to the *β*-C–H bond.[38] Consequently, if this difference in bond stability is sustained on the surface, it would favor the formation of *meso-meso* linked units in a first step followed by interconversion via strain-facilitated dehydrogenation to the triply fused motif 1.[65] In addition, the preferential *meso* C–H dehydrogenation would hinder the formation of *β-β* singly linked units (motif 3*). Furthermore, motifs 2 and 3, demanding the dehydrogenation of *β* carbons, become more prominent at higher temperatures, consistent with the order in bond stability. The second explanation is also based on a two-step mechanism: when a dimer stabilized by motif 3* is formed, one of the constituting units can rotate around the newly formed C–C bond, i.e. "folding" toward a planar configuration, bringing the four adjacent unreacted C–H bonds to close proximity and yielding a straight dimer (motif 1) via a cyclodehydrogenation process.[65] As an alternative pathway, motif 3* might also be transformed to motif 3 by rotation in an in-plane direction.

Both mechanisms imply a liftoff of the porphine units from the surface either during the *meso-meso* bond formation or the folding process. This assumption is realistic, as the 2H-P desorption readily happens at the applied substrate temperature.

In the following, we will discuss some implications of the data for both approaches introduced above regarding the reaction mechanism. It has to be emphasized that no oligomers were observed at substrate temperatures T_S below 470 K, irrespective of the evaporation temperature T_{cru}. Thus, the reaction occurs necessarily on the surface and is associated with its catalytic activity (note for comparison that the C–H bond cleavage energy under vacuum amounts to 4.5 eV[66]). Two parameters, namely the substrate temperature T_S and the molecular density, play a crucial role. First, a high density of 2H-P monomers on the surface facilitates oligomerization, in line with a recent report on dehydrogenative polymerization of heteroatomic hydrocarbons.[67] In the second approach, the time-integrated density of 2H-P monomers in a given surface region can be controlled via the continuous supply of porphines and T_S, while it is strictly limited by monomer desorption in the first approach. Second, with higher temperature T_S extended oligomers, demanding multiple dehydrogenation events per porphine unit, and coupling motif 3, requiring a dehydrogenation of two adjacent *β*-C positions (see Figure 1f), become more frequent.

Generally, eliminative on-surface reactions are described by multistep mechanisms, involving an initial dehalogenation or dehydrogenation of monomers, followed by diffusion of the resulting surface-supported radicals and subsequent coupling.[29,31,47,68] Alternatively, the two steps of the reaction (dehydrogenation and coupling) can be intimately related.[51,69] Nevertheless, the prevalence of the triply fused motif 1 at all temperatures T_S, the increasing probability for motif 3 with higher T_S and the limitation of our first approach, despite going through a monomer coverage of 1 ML during the annealing procedure, are all consistent with a multistep reaction mechanism.[51,69] Therefore, all molecules should be dehydrogenated at one or more positions after heating to a certain temperature. Since unreacted and deprotonated 2H-P molecules show no clear difference in STM data (see Figure SI 3 (Supporting Information)), this assumption cannot be disentangled directly.

However, to go beyond speculations, a massive theoretical modeling effort including the metallic support would be mandatory to clarify the details of the homocoupling reaction pathway,[34,65,69] which is beyond the scope of this article.

dx.doi.org/10.1021/ja501680n | J. Am. Chem. Soc. 2014, 136, 9346–9354

Interestingly, in a gas-phase environment, the oligomerization reaction of two porphines to yield a triply fused dimer is calculated to be isothermal, while the further extension to a trimer is exothermic.[62]

Importantly, our results show that, beyond its role as a support, the Ag(111) surface allows for an efficient diffusion of the monomers and facilitates the oligomerization of porphines, at variance with, for example, the Cu(111)[37] or Cu(100)[35] surfaces. Thus, our study confirms the ability of noble metal surfaces to catalyze chemical reactions on the basis of C−H or N−H bond cleavage.[30,35,47,51,65,67,68,70−74]

Electronic Structure and Physical Properties. In the following, we will corroborate our assignment of the observed extended porphine agglomerates to covalently linked oligomers. First, the stability of the oligomers was tested by STM manipulation. To this end, a voltage pulse of −2 V was applied at the center of one of the constituting units of a dimer to induce a lateral displacement. Figure 3 shows a dimer before (a) and after (c) a pulse. As underlined by the superposition of the two images shown in Figure 3b (red, initial state; green, final state) the dimer moved as an entity, which highlights the stability of the bond. Similar STM manipulation procedures were reported for robust supramolecules stabilized by multiple hydrogen bonds or covalent or metal−organic interactions.[29,75,76] This manipulation process was also applied to longer oligomers and resulted in a concerted translation of the entire assembly, in line with covalent bonding.

Second, space-averaging techniques (NEXAFS, UPS, XPS) were applied to comprehensively characterize the oligomeric samples and to verify the differences in the phase consisting solely of 2H-P monomers. The photoemission results, clarifying the electronic and chemical structure of the oligomers, will be discussed below. We first describe NEXAFS measurements addressing structural aspects, focusing on the angle-dependent C K-edge spectra of a sub-ML coverage of porphines (Figure 4). Details of the simulated NEXAFS spectra highlighting the particular contribution of specific molecular moieties are shown in Figure SI 4 (Supporting Information). The changes observed in the unoccupied states probed by NEXAFS upon dimerization are considerable. For the case of room-temperature deposition yielding 2H-P monomers, the sub-ML spectra are very similar to those of the 2H-P multilayer,[36] thus pointing to a weak modification induced by the minor charge transfer through interaction with the Ag(111) substrate. Consistently, the calculated C K-edge spectrum of an unsupported 2H-P molecule (Figure 4g) agrees well with the magic angle curve (53° curve, Figure 4c, red dashed line and Figure 4e) measured at sub-ML coverage (Figure 4c). For porphine deposited on the heated Ag(111) substrate (T_S = 613 K, 97% of all molecules are bound in oligomers), the experimental spectra (Figure 4d) differ substantially from those of the room-temperature preparation (Figure 4c). While the angular dependence is similar, the number of peaks is reduced with a most noticeable quenching of the first peak. This behavior has often been interpreted as an indication of electron charge transfer from the Ag surface to the adsorbate,[37,77] resulting in a (partial) filling of the lowest unoccupied molecular orbital (LUMO). However, in the present case the DFT calculations for the triply fused dimer (Figure 4h), which were conducted without including the effect of the supporting substrate, very well reproduce the experimental data (Figure 4f). This provides a strong indication that the observed NEXAFS spectra are indeed the signature of new oligomeric species resulting from covalent C−C bonds and

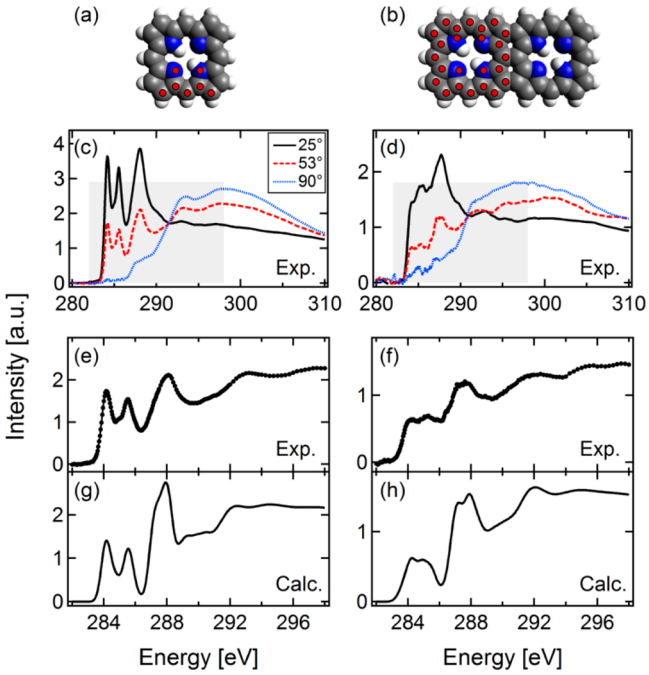

Figure 4. Experimental and simulated C K-edge NEXAFS spectra of 2H-P deposited on the Ag(111) substrate kept at room temperature (left panels) and at 613 K (right panels). Red dots in the structural models of the porphine monomer (a) and dimer (b) denote the inequivalent C and N atoms which were taken into account for the calculations (C, N, and H atoms are indicated in gray, blue, and white, respectively). Angle-resolved spectra (c, d) indicate a flat adsorption geometry. The gray areas in (c) and (d) illustrate the zoomed-in region shown in (e) and (f). The good agreement with the respective simulated spectra (g and h) shows that the modified NEXAFS signatures are a consequence of the different chemical species rather than that of a modified adsorbate−substrate interaction.

not those of a 2H-P with a modified molecule−substrate interaction. Furthermore, the vanishing intensity of the π^* resonances in the 90° curve (blue, dotted line) in both the monomeric (Figure 4c) and oligomeric (Figure 4d) samples clearly indicates a flat adsorption geometry.[36] It should be noted that the bonding represented by motif 1 prevails on the surface after preparation at T_S = 613 K (see Table 1). Nevertheless, the calculations based on a triply fused dimer (Figure 4b) are an approximation for the experimental situation, where also the other motifs in extended oligomers contribute to the space-averaged NEXAFS data.

In order to elucidate the electronic structure of the oligomers, local techniques (STM and dI/dV mapping) were complemented by space-averaging UPS experiments and theoretical modeling (extended Hückel and DFT). In the following, the discussion focuses on the dimer based on motif 1, as it represents the prevalent species adsorbed on the surface upon preparation at T_S = 573 K. STM imaging already reveals a distinct electronic structure of dimers or longer oligomers vs monomers (Figures 1b and 5a): at specific bias voltages, the apparent heights for monomers and dimers can be clearly discriminated. As this modified contrast is bias-dependent, it is assigned to a difference in electronic structure (in agreement with the NEXAFS data) rather than topography. In agreement with previously reported dI/dV spectra on 2H-P/Ag(111),[36] no distinct electronic resonances could be resolved in dI/dV spectra, presumably due to a severe broadening induced by

dx.doi.org/10.1021/ja501680n | J. Am. Chem. Soc. 2014, 136, 9346−9354

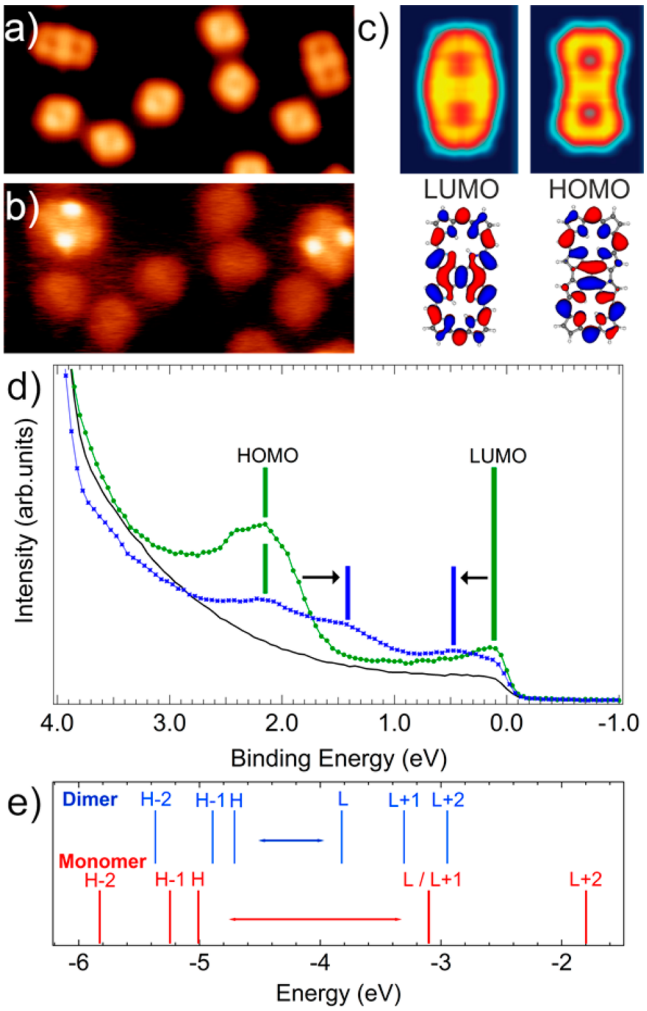

Figure 5. Electronic states of a dimer. (a) STM topography and (b) dI/dV map at −450 mV bias representing the same area on the surface (tunneling current 0.21 nA, size 11 × 5.3 nm^2). (c) STM images obtained by Hückel calculations and Kohn−Sham frontier orbitals (HOMO and LUMO) of the symmetric porphine dimer. The shapes of the orbitals agree well with those obtained from STM measurements and Hückel simulations. (d) UPS spectra recorded in grazing emission geometry for a pure porphine layer deposited at room temperature (green curve) and a reacted porphine film following surface exposure at 573 K (blue curve). The spectrum of the clean Ag(111) surface (black line) is shown for comparison. The arrows highlight the shift in opposite directions of the HOMO and LUMO states upon oligomerization. (e) DFT ground state calculation of the Kohn−Sham energies for the porphine dimer (blue) and monomer (red). The dimerization leads to a splitting of the degenerate LUMO (L) and LUMO+1 (L+1) orbitals of the monomer. In comparison to the monomer, the electronic gap between the HOMO (H) and LUMO is substantially reduced for the dimer.

interaction with the substrate. However, Figure 5b shows a dI/dV map recorded simultaneously with the STM image in Figure 5a. It represents occupied electronic states and evidences pronounced features for the triply fused dimers, characterized by two protrusions located on the connecting axis in the middle of the dimers, while the monomers show no pronounced intramolecular contrast in the dI/dV map. The spectral signature characteristic for the dimers, which is attributed to the LUMO orbital (vide infra), is relatively broad in energy. It dominates the dI/dV data in a voltage range from −0.55 V up to close to the Fermi level (see Figure SI 5 (Supporting Information)).

Further insight into the electronic structure was gained by UPS measurements, which probed the occupied electronic states located close to the Fermi level of the substrate. Figure 5d presents two representative spectra for a porphine layer deposited at T_S = 300 K (green curve) and a porphine layer deposited at 573 K (blue curve), which—according to the STM characterization of similarly prepared layers—contain predominantly monomers and covalently bonded oligomers (80%), respectively. As discussed in ref 36, the broad structure at ∼2.2 eV binding energy of the room-temperature deposited layer is ascribed to the highest occupied molecular orbital (HOMO) of individual porphine molecules, while the weaker feature crossing the Fermi level signals the partial filling of LUMO due to charge transfer from the silver substrate. Deposition at high temperature causes dramatic changes in the valence band region, the most striking being the appearance of two new states at ∼1.5 and 0.5 eV below the Fermi level. These can be naturally interpreted as arising from a shift to lower/higher binding energy, respectively, of the HOMO/LUMO of the monomers upon formation of the covalent bonds between adjacent molecules,[78] which leads to a reduction of the band gap. It has to be emphasized that UPS, as a space-averaging technique, probes a sample where considerable amounts of monomers and oligomers beyond dimers are present on the surface (Figure 2b). Hence, the spectroscopic feature at 2.2 eV is also present in the spectrum of the oligomeric sample.

These findings, namely the reduction of the electronic HOMO−LUMO gap, are not unexpected, as the gap is known to decrease for increasing oligomer lengths.[62,78−81] This reduction is also predicted by DFT ground state calculations for the porphine monomer and dimer, as shown in Figure 5e. Although the absolute gap values are not well reproduced by standard DFT calculations (e.g. ref 82), the observed trend (a reduction in the band gap for the dimer; Figure 5e, top) agrees well with the conclusions from the presented UPS measurements. Similarly, extended Hückel calculations (EHT) mimicking STM images[83] (Figure 5c) of isolated dimers support the conclusions drawn above. The top panel in Figure 5c shows simulated images based on the LUMO (left) and HOMO (right) charge density contours, respectively. The former qualitatively agrees very well with the experimental STM image of the dimer (Figure 5a). The LUMO orbital is predicted to have a significant density of states in the central part of the molecule (bottom panel in Figure 5c), in good accordance with the bright features observed in Figure 5b. The calculated constant charge density contour based on the HOMO orbital, on the other hand, is characterized by a neck in the middle of the dimer, in disagreement with the STM data. The match of the STM data in Figure 5a representing occupied electronic states with the simulated image based on the LUMO of an isolated dimer gives another hint that on the surface the LUMO is at least partially shifted below the Fermi level, resulting in a considerable filling of this orbital. This finding corroborates the experimental UPS data and is in line with the reduced electronic gap indicated by DFT. In addition, spectroscopic measurements by XPS were performed and compared to calculated spectra for a freestanding porphine molecule and a covalently linked dimer (see the Supporting Information). The theoretical calculations predict only a small shift in binding energy for the XP spectra, which is confirmed by the experiments (Figure SI 6 (Supporting Information)).

dx.doi.org/10.1021/ja501680n | J. Am. Chem. Soc. 2014, 136, 9346−9354

CONCLUSION

We introduced an in situ covalent dehydrogenative coupling mechanism yielding covalent porphine aggregates directly on a noble metal surface in a highly controlled UHV environment without any byproducts left on the surface. The resulting nanostructures range from highly symmetric triply fused porphine dimers to irregular oligomers exceeding 90 porphine units, as controlled by the experimental conditions. Our multitechnique approach combining STM, dI/dV mapping, NEXAFS, UPS, XPS, and complementary extended Hückel and DFT calculations demonstrates the surface-assisted, temperature-induced formation of C−C bonds and includes the comprehensive characterization of the resulting oligomers with submolecular precision. In addition, it evidences striking differences in the electronic band gap and the frontier orbitals of surface anchored oligomers and monomers. Although these physical property changes were predictable for isolated species, we directly demonstrate their existence and exquisite details for units supported on a metallic substrate, rendering elements with prospects for nanoelectronic or photophysical applications. Thus, we present the products of dehydrogenative homocoupling reactions with direct access to their physical properties which can be characterized with high precision at the molecular level. Our results open new bottom-up pathways for the construction of covalent porphyrin nanoarchitectures exhibiting tailored electronic properties. Specifically, (partially) metalated dimers or trimers present particularly interesting model systems to study the coupling of different metallic centers in a macrocyclic environment or introduce potential elements for molecular memory units.[84] Furthermore, a new protocol featuring porphine deposition on a heated Ag(111) surface drastically increased the oligomer coverage and extension, an effect attributed to the decisive role of the total amount of monomers in the surface region. In summary, our results introduce a simple approach to surface-supported covalent porphine aggregates in a clean environment, which cannot be achieved by conventional means, such as sublimation. As a perspective, template-guided homocoupling protocols might yield an improved control of the reaction products.[85] The presented single-step bottom-up method will serve as a basis for the exploration of more elaborate porphine architectures in the future, targeting a systematic tailoring of their geometry as well as chemical and physical properties.

ASSOCIATED CONTENT

Supporting Information

Figures and text giving additional STM data, X-ray photoelectron spectra, and details of the calculations. This material is available free of charge via the Internet at http://pubs.acs.org.

AUTHOR INFORMATION

Corresponding Author

*E-mail for W.A.: wau@tum.de.

Present Addresses

[⊥]Institut für Chemie, Karl-Franzens-Universität Graz, 8010 Graz, Austria.

[#]IMDEA Nanoscience, 28049 Madrid, Spain.

[$]Department Chemie, Technische Universität München, Lichtenbergstraße 4, D-85748 Garching, Germany.

Notes

The authors declare no competing financial interest.

ACKNOWLEDGMENTS

This work was supported by the ERC Advanced Grant MolArt (No. 247299), the Munich Center for Advanced Photonics (MAP), and the Technische Universität München-Institute for Advanced Study, funded by the German Research Foundation (DFG) via the German Excellence Initiative. A.C.P. was supported by a Marie Curie Intra-European Fellowship (project NASUMECA, No. 274842). We thank the Helmholtz-Zentrum Berlin-Electron storage ring BESSY II for provision of synchrotron radiation at beamline HE-SGM and traveling support. We also thank ELETTRA for providing synchrotron radiation and Kevin C. Prince for support and useful discussion during the experiments at the Materials Science Beamline. We thank D. Stassen (Université de Namur) for helpful discussions. A.W. acknowledges support by the International Max Planck Research School of Advanced Photon Science (IMPRS-APS). T.H. Ngo acknowledges support by the International Center for Young Scientists (ICYS) and the International Center for Materials Nanoarchitectonics (MANA).

REFERENCES

(1) Wolff, J. B.; Price, L. *Arch. Biochem. Biophys.* **1957**, *72*, 293.
(2) Perutz, M. F. *Nature* **1970**, *228*, 726.
(3) Collman, J. P.; Boulatov, R.; Sunderland, C. J.; Fu, L. *Chem. Rev.* **2004**, *104*, 561.
(4) Lin, V. S.-Y.; DiMagno, S. G.; Therien, M. J. *Science* **1994**, *264*, 1105.
(5) Jung, T. A.; Schlittler, R. R.; Gimzewski, J. K. *Nature* **1997**, *386*, 696.
(6) Wojaczynski, J.; Latos-Grazynski, L. *Coord. Chem. Rev.* **2000**, *204*, 113.
(7) Tsuda, A.; Osuka, A. *Science* **2001**, *293*, 79.
(8) Elemans, J. A. A. W.; van Hameren, R.; Nolte, R. J. M.; Rowan, A. E. *Adv. Mater.* **2006**, *18*, 1251.
(9) Auwärter, W.; Weber-Bargioni, A.; Brink, S.; Riemann, A.; Schiffrin, A.; Ruben, M.; Barth, J. V. *ChemPhysChem* **2007**, *8*, 250.
(10) Barth, J. V. *Annu. Rev. Phys. Chem.* **2007**, *58*, 375.
(11) Auwärter, W.; Seufert, K.; Klappenberger, F.; Reichert, J.; Weber-Bargioni, A.; Verdini, A.; Cvetko, D.; Dell'Angela, M.; Floreano, L.; Cossaro, A.; Bavdek, G.; Morgante, A.; Seitsonen, A. P.; Barth, J. V. *Phys. Rev. B* **2010**, *81*, 245403.
(12) Makiura, R.; Kitagawa, H. *Eur. J. Inorg. Chem.* **2010**, *2010*, 3715.
(13) Mohnani, S.; Bonifazi, D. *Coord. Chem. Rev.* **2010**, *254*, 2342.
(14) Seufert, K.; Bocquet, M.-L.; Auwärter, W.; Weber-Bargioni, A.; Reichert, J.; Lorente, N.; Barth, J. V. *Nat. Chem.* **2011**, *3*, 114.
(15) Lindsey, J. S.; Bocian, D. F. *Acc. Chem. Res.* **2011**, *44*, 638.
(16) Yella, A.; Lee, H.-W.; Tsao, H. N.; Yi, C.; Chandiran, A. K.; Nazeeruddin, M. K.; Diau, E. W.-G.; Yeh, C.-Y.; Zakeeruddin, S. M.; Grätzel, M. *Science* **2011**, *334*, 629.
(17) Li, L.-L.; Diau, E. W.-G. *Chem. Soc. Rev.* **2013**, *42*, 291.
(18) Zimmerman, J. D.; Diev, V. V.; Hanson, K.; Lunt, R. R.; Yu, E. K.; Thompson, M. E.; Forrest, S. R. *Adv. Mater.* **2010**, *22*, 2780.
(19) Naoda, K.; Mori, H.; Aratani, N.; Lee, B. S.; Kim, D.; Osuka, A. *Angew. Chem. Int. Ed* **2012**, *51*, 9856.
(20) Biggs, J. D.; Zhang, Y.; Healion, D.; Mukamel, S. *Proc. Natl. Acad. Sci. U.S.A.* **2013**, *110*, 15597.
(21) Li, E. Y.; Marzari, N. *J. Phys. Chem. Lett.* **2013**, *4*, 3039.
(22) Nguyen, T. Q.; Sison Escaño, M. C.; Shimoji, N.; Nakanishi, H.; Kasai, H. *Phys. Rev. B* **2008**, *77*, 195307.
(23) Cho, H. S.; Jeong, D. H.; Cho, S.; Kim, D.; Matsuzaki, Y.; Tanaka, K.; Tsuda, A.; Osuka, A. *J. Am. Chem. Soc.* **2002**, *124*, 14642.
(24) Kim, D. Y.; Ahn, T. K.; Kwon, J. H.; Kim, D.; Ikeue, T.; Aratani, N.; Osuka, A.; Shigeiwa, M.; Maeda, S. *J. Phys. Chem. A* **2005**, *109*, 2996.
(25) Takagi, A.; Yanagawa, Y.; Tsuda, A.; Aratani, N.; Matsumoto, T.; Osuka, A.; Kawai, T. *Chem. Commun.* **2003**, 2986.

(26) Nakamura, Y.; Aratani, N.; Shinokubo, H.; Takagi, A.; Kawai, T.; Matsumoto, T.; Yoon, Z. S.; Kim, D. Y.; Ahn, T. K.; Kim, D.; Muranaka, A.; Kobayashi, N.; Osuka, A. *J. Am. Chem. Soc.* **2006**, *128*, 4119.
(27) Bonifazi, D.; Spillmann, H.; Kiebele, A.; de Wild, M.; Seiler, P.; Cheng, F.; Güntherodt, H.-J.; Jung, T.; Diederich, F. *Angew. Chem., Int. Ed.* **2004**, *43*, 4759.
(28) Krasnikov, S. A.; Sergeeva, N. N.; Sergeeva, Y. N.; Senge, M. O.; Cafolla, A. A. *Phys. Chem. Chem. Phys.* **2010**, *12*, 6666.
(29) Grill, L.; Dyer, M.; Lafferentz, L.; Persson, M.; Peters, M. V.; Hecht, S. *Nat. Nano.* **2007**, *2*, 687.
(30) Veld, M. I.; Iavicoli, P.; Haq, S.; Amabilino, D. B.; Raval, R. *Chem. Commun.* **2008**, 1536.
(31) Lafferentz, L.; Eberhardt, V.; Dri, C.; Africh, C.; Comelli, G.; Esch, F.; Hecht, S.; Grill, L. *Nat. Chem.* **2012**, *4*, 215.
(32) Lin, T.; Shang, X. S.; Adisoejoso, J.; Liu, P. N.; Lin, N. *J. Am. Chem. Soc.* **2013**, *135*, 3576.
(33) Dyer, M. S.; Robin, A.; Haq, S.; Raval, R.; Persson, M.; Klimes, J. *ACS Nano* **2011**, *5*, 1831.
(34) Hanke, F.; Haq, S.; Raval, R.; Persson, M. *ACS Nano* **2011**, *5*, 9093.
(35) Haq, S.; Hanke, F.; Dyer, M. S.; Persson, M.; Iavicoli, P.; Amabilino, D. B.; Raval, R. *J. Am. Chem. Soc.* **2011**, *133*, 12031.
(36) Bischoff, F.; Seufert, K.; Auwärter, W.; Joshi, S.; Vijayaraghavan, S.; Ecija, D.; Diller, K.; Papageorgiou, A. C.; Fischer, S.; Allegretti, F.; Duncan, D. A.; Klappenberger, F.; Blobner, F.; Han, R.; Barth, J. V. *ACS Nano* **2013**, *7*, 3139.
(37) Diller, K.; Klappenberger, F.; Allegretti, F.; Papageorgiou, A. C.; Fischer, S.; Wiengarten, A.; Joshi, S.; Seufert, K.; Ecija, D.; Auwärter, W.; Barth, J. V. *J. Chem. Phys.* **2013**, *138*, 154710.
(38) Osuka, A.; Shimidzu, H. *Angew. Chem., Int. Ed.* **1997**, *36*, 135.
(39) Ryan, A. A.; Senge, M. O. *Eur. J. Org. Chem.* **2013**, *2013*, 3700.
(40) Tagami, K.; Tsukada, M.; Matsumoto, T.; Kawai, T. *Phys. Rev. B* **2003**, *67*, 245324.
(41) Nakamura, Y.; Hwang, I. W.; Aratani, N.; Ahn, T. K.; Ko, D. M.; Takagi, A.; Kawai, T.; Matsumoto, T.; Kim, D.; Osuka, A. *J. Am. Chem. Soc.* **2004**, *127*, 236.
(42) Gao, G.; Kang, H. S. *Chem. Phys.* **2010**, *369*, 66.
(43) Klappenberger, F. *Prog. Surf. Sci.* **2014**, *89*, 1.
(44) Sakamoto, J.; Heijst, J. v.; Lukin, O.; Schlueter, A. D. *Angew. Chem., Int. Ed.* **2009**, *48*, 1030.
(45) Franc, G.; Gourdon, A. *Phys. Chem. Phys.* **2011**, *13*, 14283.
(46) Lackinger, M.; Heckl, W. M. *J. Phys. D* **2011**, *44*, 464011.
(47) Mendez, J.; Lopez, M. F.; Martin-Gago, J. A. *Chem. Soc. Rev.* **2011**, *40*, 4578.
(48) Colson, J. W.; Dichtel, W. R. *Nat. Chem.* **2013**, *5*, 453.
(49) Otero, R.; Gallego, J. M.; de Parga, A. L. V.; Martin, N.; Miranda, R. *Adv. Mater.* **2011**, *23*, 5148.
(50) Müllegger, S.; Winkler, A. *Surf. Sci.* **2006**, *600*, 3982.
(51) Zhang, Y.-Q.; Kepcija, N.; Kleinschrodt, M.; Diller, K.; Fischer, S.; Papageorgiou, A. C.; Allegretti, F.; Bjoerk, J.; Klyatskaya, S.; Klappenberger, F.; Ruben, M.; Barth, J. V. *Nat. Commun.* **2012**, *3*, 1286.
(52) Abel, M.; Clair, S.; Ourdjini, O.; Mossoyan, M.; Porte, L. *J. Am. Chem. Soc.* **2010**, *133*, 1203.
(53) Stöhr, J. *NEXAFS Spectroscopy*; Springer-Verlag: Berlin, 1992.
(54) Hermann, K.; Pettersson, L. G. M. (deMon developers group) *StoBe software V. 3.0*, 2007; see http://www.fhi-berlin.mpg.de/KHsoftware/StoBe/.
(55) Perdew, J. P.; Burke, K.; Ernzerhof, M. *Phys. Rev. Lett.* **1996**, *77*, 3865.
(56) Hammer, B.; Hansen, L. B.; Norskov, J. K. *Phys. Rev. B* **1999**, *59*, 7413.
(57) Dunning, T. H. J. *J. Chem. Phys.* **1971**, *55*, 716.
(58) Huzinaga, S. *J. Chem. Phys.* **1965**, *42*, 1293.
(59) Slater, J. C. *Adv. Quantum Chem.* **1972**, *6*, 1.
(60) Triguero, L.; Pettersson, L. G. M. *Phys. Rev. B* **1998**, *58*, 8097.
(61) *HyperChem*; Hypercube Inc., 1115 NW 4th Street, Gainesville, Florida 32601, USA.
(62) Charkin, O. P.; Klimenko, N. M. *Russ. J. Inorg. Chem.* **2013**, *58*, 1058.
(63) Lipton-Duffin, J. A.; Ivasenko, O.; Perepichka, D. F.; Rosei, F. *Small* **2009**, *5*, 592.
(64) Wang, W.; Shi, X.; Wang, S.; Van Hove, M. A.; Lin, N. *J. Am. Chem. Soc.* **2011**, *133*, 13264.
(65) Treier, M.; Pignedoli, C. A.; Laino, T.; Rieger, R.; Müllen, K.; Passerone, D.; Fasel, R. *Nat. Chem.* **2011**, *3*, 61.
(66) Streitwieser, A.; Heathcock, C. H. *Introduction to organic chemistry*; Macmillan: New York, 1985.
(67) Pinardi, A. L.; Otero-Irurueta, G.; Palacio, I.; Martinez, J. I.; Sanchez-Sanchez, C.; Tello, M.; Rogero, C.; Cossaro, A.; Preobrajenski, A.; Gomez-Lor, B.; Jancarik, A.; Stara, I. G.; Stary, I.; Lopez, M. F.; Mendez, J.; Martin-Gago, J. A. *ACS Nano* **2013**, *7*, 3676.
(68) Björk, J.; Hanke, F. *Chem. Eur. J.* **2014**, *20*, 928.
(69) Björk, J.; Zhang, Y.-Q.; Klappenberger, F.; Barth, J. V.; Stafström, S. *J. Phys. Chem. C* **2014**, *118*, 3181.
(70) Di Santo, G.; Blankenburg, S.; Castellarin-Cudia, C.; Fanetti, M.; Borghetti, P.; Sangaletti, L.; Floreano, L.; Verdini, A.; Magnano, E.; Bondino, F.; Pignedoli, C. A.; Nguyen, M.-T.; Gaspari, R.; Passerone, D.; Goldoni, A. *Chem. Eur. J.* **2011**, *17*, 14354.
(71) Heinrich, B. W.; Ahmadi, G.; Müller, V. L.; Braun, L.; Pascual, J. I.; Franke, K. J. *Nano Lett.* **2013**, *13*, 4840.
(72) Papageorgiou, A. C.; Fischer, S.; Oh, S. C.; Saglam, O.; Reichert, J.; Wiengarten, A.; Seufert, K.; Vijayaraghavan, S.; Ecija, D.; Auwärter, W.; Allegretti, F.; Acres, R. G.; Prince, K. C.; Diller, K.; Klappenberger, F.; Barth, J. V. *ACS Nano* **2013**, *7*, 4520.
(73) Weigelt, S.; Schnadt, J.; Tuxen, A. K.; Masini, F.; Bombis, C.; Busse, C.; Isvoranu, C.; Ataman, E.; Lægsgaard, E.; Besenbacher, F.; Linderoth, T. R. *J. Am. Chem. Soc.* **2008**, *130*, 5388.
(74) Zhong, D.; Franke, J.-H.; Podiyanachari, S. K.; Blömker, T.; Zhang, H.; Kehr, G.; Erker, G.; Fuchs, H.; Chi, L. *Science* **2011**, *334*, 213.
(75) Heim, D.; Écija, D.; Seufert, K.; Auwärter, W.; Aurisicchio, C.; Fabbro, C.; Bonifazi, D.; Barth, J. V. *J. Am. Chem. Soc.* **2010**, *132*, 6783.
(76) Nickel, A.; Ohmann, R.; Meyer, J.; Grisolia, M.; Joachim, C.; Moresco, F.; Cuniberti, G. *ACS Nano* **2012**, *7*, 191.
(77) Tseng, T.-C.; Urban, C.; Wang, Y.; Otero, R.; Tait, S. L.; Alcama, M.; Ecija, D.; Trelka, M.; Gallego, J. M.; Lin, N.; Konuma, M.; Starke, U.; Nefedov, A.; Langner, A.; Woell, C.; Herranz, M. A.; Martin, F.; Martin, N.; Kern, K.; Miranda, R. *Nat. Chem.* **2010**, *2*, 374.
(78) Cardenas, L.; Gutzler, R.; Lipton-Duffin, J.; Fu, C.; Brusso, J. L.; Dinca, L. E.; Vondracek, M.; Fagot-Revurat, Y.; Malterre, D.; Rosei, F.; Perepichka, D. F. *Chem. Sci.* **2013**, *4*, 3263.
(79) Zade, S. S.; Bendikov, M. *Org. Lett.* **2006**, *8*, 5243.
(80) Zade, S. S.; Zamoshchik, N.; Bendikov, M. *Acc. Chem. Res.* **2011**, *44*, 14.
(81) Yamaguchi, Y. *J. Chem. Phys.* **2002**, *117*, 9688.
(82) Dabo, I.; Ferretti, A.; Park, C.-H.; Poilvert, N.; Li, Y.; Cococcioni, M.; Marzari, N. *PhysChemPhys* **2013**, *15*, 685.
(83) Auwärter, W.; Weber-Bargioni, A.; Riemann, A.; Schiffrin, A.; Gröning, O.; Fasel, R.; Barth, J. V. *J. Chem. Phys.* **2006**, *124*, 194708.
(84) Yokoyama, T.; Nishiyama, F. *J. Phys. Chem. Lett.* **2014**, *5*, 1324.
(85) Cirera, B.; Zhang, Y.-Q.; Björk, J.; Klyatskaya, S.; Chen, Z.; Ruben, M.; Barth, J. V.; Klappenberger, F. *Nano Lett.* **2014**, *14*, 1891.